GEOCHEMISTRY OF SEABED AND COASTAL SEDIMENTS IN LIMAU WATERS AREA

GEOKIMIA SEDIMEN DASAR LAUT DAN PANTAI DI PERAIRAN LIMAU DAN SEKITARNYA

Muhammad Zulfikar*, Eko Saputro, Ali Albab, Riza Rahardiawan

Marine Geological Institute, Jl. Dr. Junjunan no.236, Bandung

*Corresponding author: muhammad.zulfikar@esdm.go.id

(Received 03 July 2025; in revised from 04 July 2025; accepted 29 December 2025)

DOI : 10.32693/bomg.40.2.2025.953

ABSTRACT: Sediment provenance and weathering history are used to understand sedimentary processes and to explore mineral potential in coastal–marine systems in the Limau Waters. Therefore, the characteristics of seabed and coastal sediments need to be determined. This study aims to identify the source rocks, paleoweathering signatures, and sediment maturity of both seabed and coastal sediments through a geochemical approach. A geochemical approach that integrates major oxide and rare earth element (REE) analyses, the paleoweathering, and sediment maturity indices, is used to identify the source rocks of these sediments. Major oxides elements were measured using X-ray fluorescence (XRF) and REE concentrations were determined using inductively coupled plasma - optical emission spectrometry (ICP-OES) and inductively coupled plasma optical - mass spectrometry (ICP-MS). Geochemical discrimination diagrams indicate that seabed sediments are mainly derived from intermediate to felsic igneous rocks with higher compositional maturity, whereas coastal sediments are influenced by mafic volcanic rocks and are comparatively immature in composition. Both sediment types exhibit weak chemical weathering (CIA < 70), suggesting limited alteration of young volcanic sources. The CIA–ICV relationships portray contrast sediment transport and depositional processes between the coastal and marine environments. This study is expected to provide a geochemical-based framework for provenance analysis and to support the development of insights for future marine mineral exploration in the Limau Waters area.

Keywords: Marine sediment geochemistry, provenance analysis, chemical weathering, Limau Waters

ABSTRAK: *Asal usul sedimen dan sejarah pelapukan digunakan untuk memahami proses sedimentasi dan mengeksplorasi potensi mineral di sistem pesisir-laut Perairan Limau. Oleh karena itu, perlu dilakukan penentuan karakteristik pada sedimen dasar laut dan pesisir. Penelitian ini bertujuan untuk mengidentifikasi batuan sumber, jejak pelapukan purba, dan tingkat kematangan sedimen pada sedimen dasar laut maupun sedimen pantai melalui pendekatan geokimia. Pendekatan geokimia yang mengintegrasikan analisis unsur oksida utama dan unsur tanah jarang (UTJ), pelapukan purba, serta indeks kematangan sedimen, digunakan untuk mengidentifikasi batuan sumber sedimen. Unsur oksida utama diukur dengan menggunakan fluoresensi sinar-X (XRF), sedangkan konsentrasi UTJ ditentukan dengan menggunakan ICP-OES dan ICP-MS. Diagram diskriminasi geokimia, menunjukkan bahwa sedimen dasar laut sebagian besar berasal dari batuan beku intermediet hingga felsik dengan kematangan komposisi yang lebih tinggi, sementara sedimen pantai dipengaruhi oleh batuan vulkanik mafik yang berkomposisi relatif belum matang. Kedua jenis sedimen tersebut menunjukkan pelapukan kimiawi yang lemah (CIA < 70), yang terlihat dari adanya proses alterasi terbatas pada sumber batuan vulkanik muda. Hubungan CIA-ICV menggambarkan kekontrasan transpor sedimen dan*

proses pengendapan pada lingkungan pesisir dan laut. Studi ini diharapkan dapat memberikan kerangka kerja analisis provenans dengan menggunakan data geokimia dan mendukung pengembangan wawasan dalam kegiatan eksplorasi mineral kelautan di Perairan Limau pada masa yang akan datang.

Kata Kunci: *Geokimia sedimen laut, analisis provenans, pelapukan kimia, Perairan Limau*

INTRODUCTION

Limau Waters is a shallow marine area in Tanggamus, South Lampung, that hosts potential occurrences of economic minerals such as gold placer deposits (Darlan, 1997; Sukardjono et al., 1990) and zeolite (Muksin & Heditama, 2016). The presence of these minerals in southern Lampung is associated with the Sumatran fault system, particularly the segment within the Kotaagung and its surroundings. Geologically, the area is composed of the Oligo–Miocene volcanic rocks, dominated by andesite and dacite. Primary gold deposits occur as quartz vein orebodies formed by low-sulphidation epithermal Au–Ag mineralization, while secondary deposits are represented by ancient placer deposits (Crow & Van Leeuwen, 2005).

According to Irzon (2020), lithological units distributed along the coastal regions of Kotaagung and Limau are predominantly Quaternary and Tertiary volcanic rocks. The Tertiary units consist of basaltic trachyandesite, trachyandesite, dacite, and rhyolite, whereas the Quaternary volcanic rocks comprise basalt, basaltic andesite, and andesite. Despite this geological framework, no specific studies have yet focused on the provenance of seabed and coastal sediments in the Limau Waters area.

This study therefore aims to identify the source rocks, paleoweathering signatures, and sediment maturity of both seabed and coastal sediments through a geochemical approach. The analytical framework integrates major oxide geochemistry (Cruz et al., 2021; Cullers, 1994; Roser & Korsch, 1988) and rare earth element (REE) concentrations (Cruz et al., 2021; Ekoa Bessa et al., 2021; Sousa et al., 2022; McLennan, 1989). A clearer understanding of sediment provenance would provide valuable insights for future exploration of mineral-bearing source rocks in Limau Waters and the surrounding region.

Physiography and Geological Setting of Lampung Area and Surroundings

Sumatera Island was formed from the meeting of three terranes, namely: Sibumasu, West Sumatra, and Woyla (Barber & Crow, 2005; Metcalfe, 2017). The Sibumasu was a part of Gondwana that moved relatively northward in the Early Permian which then collided with the West Sumatra in the Late Permian (Barber & Crow, 2005). There was a change in subduction from Cathaysia to the Sibumasu due to the subduction of the Mesotethys Ocean Plate which Advokaat et al. (2018) called the Ngalau Ocean Plate. The formation of the Mid Oceanic Ridge (MOR) on the Ngalau Ocean Plate which was tilted towards subduction caused the formation of a right-hand horizontal fault which caused the West Sumatra to move relatively westward so that the Sibumasu was sandwiched between two terranes associated with Cathaysia (Barber & Crow, 2005).

The stratigraphic framework of the study area generally comprises Tertiary and Quaternary rock units (Amin, 1993). From oldest to youngest, the succession begins with the Hulusimpang Volcanic Rocks Formation (Tomh) of Oligocene–Early Miocene age, characterized by volcanic breccia, lava flows, and andesitic–basaltic tuff. Much of this unit exhibits hydrothermal alteration, which has resulted in the development of quartz veins hosting sulfide minerals. Conformably overlying this formation is the Seblat Sedimentary Rocks Formation (Toms), dated to the Oligocene–Middle Miocene. Its lithology consists of interbedded mudstone, sandstone, tuffaceous sandstone, shale, and calcareous siltstone, locally accompanied by thin limestone beds or nodules.

The stratigraphy continues upward with the Bal Volcanic Rocks Formation (Tmba) of Middle–Late Miocene age, which lies conformably above both the Hulusimpang and Seblat Formations. This unit is dominated by dacitic volcanic breccia, dacite tuff, and sandstone. Emplaced within these older sequences is the Tertiary Granite/Dacite Intrusive Complex (Tmgr/Tmda), representing a Middle Miocene magmatic event. The intrusion consists of felsic plutonic rocks that cut across the Hulusimpang, Seblat, and Bal Formations. Overlying these units is the Simpangaur Sedimentary Rocks Formation (Tmps) of Pliocene age, comprising tuffaceous sandstone, tuffaceous siltstone, tuff, and polymict conglomerate. This formation also contains molluscan macrofossils, shell fragments, and locally

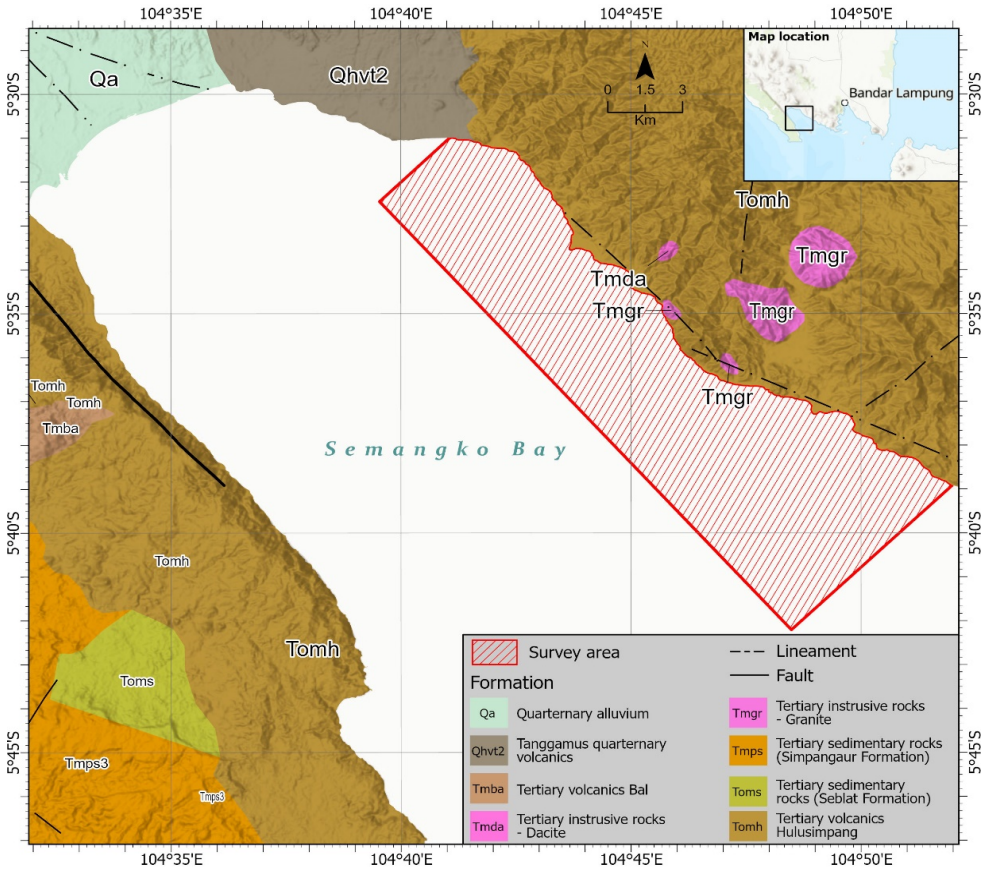

Figure 1. Tanggamus and surroundings area geological map (Modified from Amin, 1993)

thin lignite layers, indicating deposition in a shallow-marine to deltaic environment.

The youngest volcanic unit in the area is the Tanggamus Quaternary Volcanic Rocks (Qhvt), deposited during the Pleistocene–Holocene and sourced from Mount Tanggamus. It consists of volcanic breccia, lava flows, and andesite–basalt tuff. The stratigraphic sequence is capped by Quaternary Alluvium (Qa), an unconsolidated Holocene deposit composed of boulders, gravel, pebbles, sand, silt, clay, and mud, typically accumulated within estuarine and active fluvial environments under ongoing modern sedimentation.

METHODS

Sampling method

The sediment sampling was divided into two parts, namely: coastal sediment sampling and seabed sediment sampling. Seabed sediment sampling used a survey vehicle of a local fishing boat equipped with supporting equipment in the form of a set of navigation tools, winch and grab samplers. The location of the sample points had been determined at intervals of around 1-4 km with a maximum seabed depth of about 80 meters. The seabed depth levels below could not be taken due to limited sampling equipment. Meanwhile, coastal sediment samples were taken by hand auger sediment sampler (Figure 2). The location of the sample points had been determined at intervals of about 1-3 km by considering changes in coastal sediment characteristics in the field.

Sampling activities for collecting seabed samples were carried out by heading towards the planned sampling points, then taken using a grab sampler and winch 2-6 times. After the sediment sample had been successfully taken, the sample was then put into an airtight sample plastic and labeled. A total of 44 samples was taken, consisting of fine fraction sediment (~60–70%) and sand fraction sediment (~30–40%).

Coastal sediment sampling activities were carried out by heading toward the predetermined sampling points. The coastal sediments were collected using a hand auger sampler, taken from approximately 10 cm below the beach surface, and immediately placed into airtight plastic bags, which were then labeled for laboratory analysis. A total of 18 coastal sediment samples were collected, predominantly composed of the sand fraction. Figure 3 shows the 62 sediment samples (both marine and

Figure 2. Coastal sediment sampling with hand auger

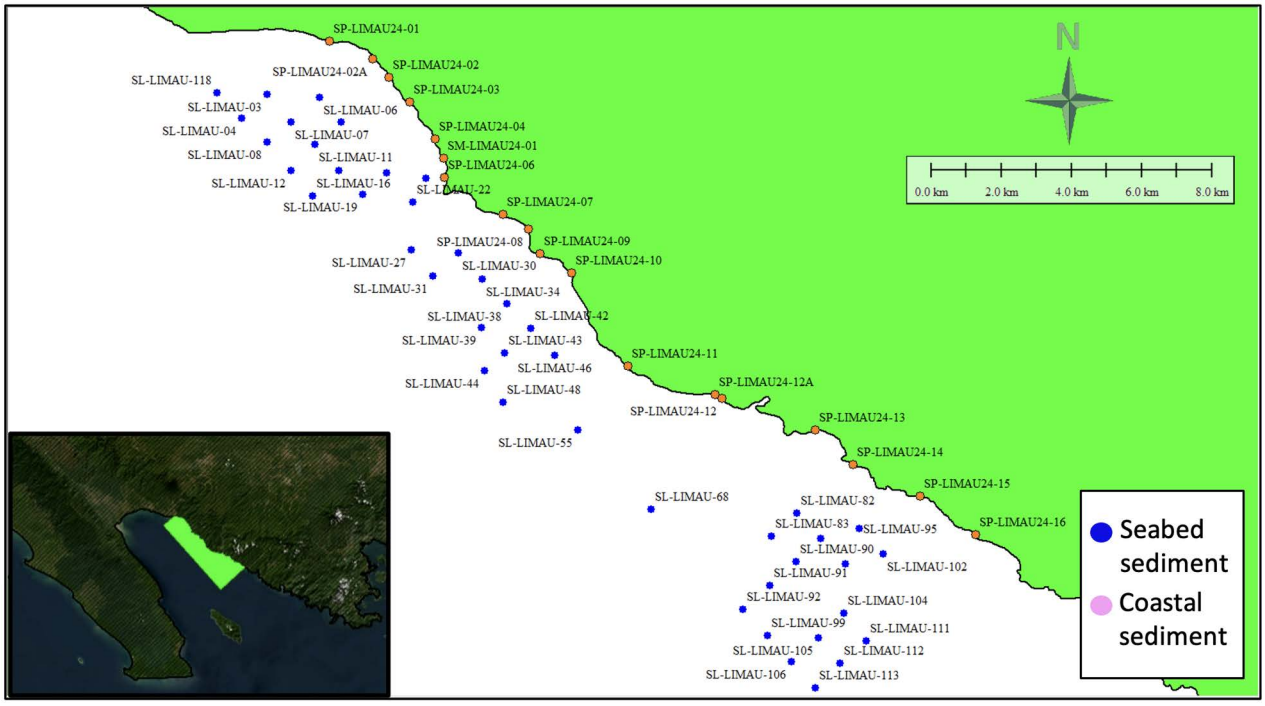

Figure 3. Seabed and coastal sediment sample location map

coastal sediments) collected for geochemical analysis using ICP–OES+MS and XRF.

Analytical method

Geochemical analytical methods used for this research were run by ICP-OES+MS and XRF devices. The ICP-OES+MS method was used to determine the REE content, while XRF was used to determine the content of the major oxide elements. The REE content were normalized to chondrite values. Several geochemical ratios and anomalies were calculated to evaluate REE fractionation and anomalies, including Eu, Ce, and REE enrichment ratios.

The europium anomaly (Eu/Eu*) was calculated using the equation:

$$Eu/Eu* = \frac{Eu(Sample)/Eu\ (Chondrite)}{\sqrt{\frac{Sm(Sample)}{Sm(Chondrite)}\ X\ \frac{Gd\ (Sample)}{Gd\ (Chondrite)}}} \quad (1)$$

The cerium anomaly (Ce/Ce*) was determined by:

$$Ce/Ce^* = \frac{Ce(Sample)/Ce\ (Chondrite)}{\sqrt{\frac{La\ (Sample)}{La\ (Chondrite)}\ X\ \frac{Pr\ (Sample)}{Pr\ (Chondrite)}}} \quad (2)$$

REE fractionation between light and heavy groups was expressed using normalized ratios:

$$(La/Sm)_N = \frac{La(Sample)/La\ (Chondrite)}{Sm(Sample)/Sm\ (Chondrite)} \quad (3)$$

$$(Gd/Yb)_N = \frac{Gd(Sample)/Gd\ (Chondrite)}{Yb(Sample)/Yb\ (Chondrite)} \quad (4)$$

Additionally, for describing the overall REE pattern slope we used:

$$(La/Yb)_N = \frac{La(Sample)/La\ (Chondrite)}{Yb(Sample)/Yb\ (Chondrite)} \quad (5)$$

The discriminant functions (Roser & Korsch, 1988) used to identify the source rock composition are calculated using the following equations:

$$F1 = (-1.773 \times TiO_2)+(0.607 \times Al_2O_3)+ (0.76\times Fe_2O_3) + (-1.5 \times MgO) + (0.616 \times CaO) + (0.509 \times Na_2O) + (-1.22 \times K_2O)+(-9.09). \quad (6)$$

$$F2 = (0.445 \times TiO_2) + (0.07\times Al_2O_3)+(-0.25 \times Fe_2O_3)+(-1.142 \times MgO) + (0.438 \times CaO) +(1.475 \times Na_2O) + (1.426 \times K_2O) + (-6.861) \quad (7)$$

These discriminant functions (F_1 and F_2) are used to classify the provenance of sedimentary rocks into mafic, intermediate, felsic, or quartzose sedimentary source types based on major oxide compositions. Meanwhile, the major oxide element contents are plotted into the discrimination function (Roser & Korsch, 1988) to determine the source rock, and the TiO_2 versus Zr content is used to determine the tectonic setting of the source rock formation. From all of these identification functions, information can be obtained regarding the type of source rock and its formation process.

To further evaluate the degree of chemical weathering and sediment maturity, several weathering indices were calculated, including the Chemical Index of Alteration (CIA), Plagioclase Index of Alteration (PIA), Chemical Index of Weathering (CIW), and Index of Compositional Variability (ICV), as defined by the following equations:

$$CIA\ (\%) = \frac{Al_2O_3}{(Al_2O_3+CaO^*+Na_2O+K_2O)}\ X\ 100 \text{ (Nesbit and Young, 1984)} \quad (8)$$

$$PIA\ (\%) = \frac{Al_2O_3-K_2O}{(Al_2O_3+CaO^*+Na_2O-K_2O)}\ X\ 100 \text{ (Fedo et al., 1995)} \quad (9)$$

$$CIW\ (\%) = \frac{Al_2O_3}{(Al_2O_3+CaO^*+Na_2O)}\ X\ 100 \text{ (Harnois, 1988)} \quad (10)$$

$$ICV\ (\%) = \frac{Fe_2O_3+K_2O+CaO^*+Na_2O+MgO+MnO+TiO_2}{Al_2O_3}\ X\ 100 \text{ (Cox et al., 1995)} \quad (11)$$

These indices provide quantitative measures of chemical weathering intensity and sediment compositional maturity, reflecting the paleoenvironmental and provenance conditions of the studied sediments.

RESULTS

Rare Earth Elements Contents

Results indicate that the total rare earth element (REE) concentrations in the samples range from 38 to 88.93 ppm. For geochemical classification, LREE (light rare earth elements) are defined as the light lanthanides from La to Sm, MREE (middle rare earth elements) comprise the intermediate lanthanides from Eu to Dy, and HREE (heavy rare earth elements) correspond to the heavier lanthanides from Ho to Lu.

The LREE/HREE ratios, which range from 4.41 to 8.79, demonstrate a clear enrichment of LREE relative to HREE. This is further supported by the relatively high La/Yb ratios (Table 1), ranging from 4.9 to 12.59, indicating pronounced LREE enrichment across the samples. Meanwhile, the LREE/MREE ratios, represented by La/Sm, range from 2.13 to 3.58, suggesting fractionation that favors LREE over MREE. In addition, the MREE/HREE ratios, represented by Gd/Yb, range from 1.93 to 2.57, reflecting an enrichment of MREE relative to HREE.

All the REE contents were normalized with chondrite values of McDonough and Sun (1995) to eliminate the natural fractionation patterns and to identify geological processes. Based on the chondrite-normalized REE data, different trend patterns are observed between seabed sediments (Figure 4a) and coastal sediments (Figure 4b).

Seabed sediments exhibit a positive Ce anomaly, with values ranging from 1.14 to 1.27. Conversely, the Ce anomaly in coastal sediments is typically negative or near one, ranging from 0.91 to 1.00. Positive Ce anomalies in seabed sediments may reflect stable open-marine depositional conditions with limited detrital input (Anenburg & Liu, 2024; Zhang & Shields, 2022).

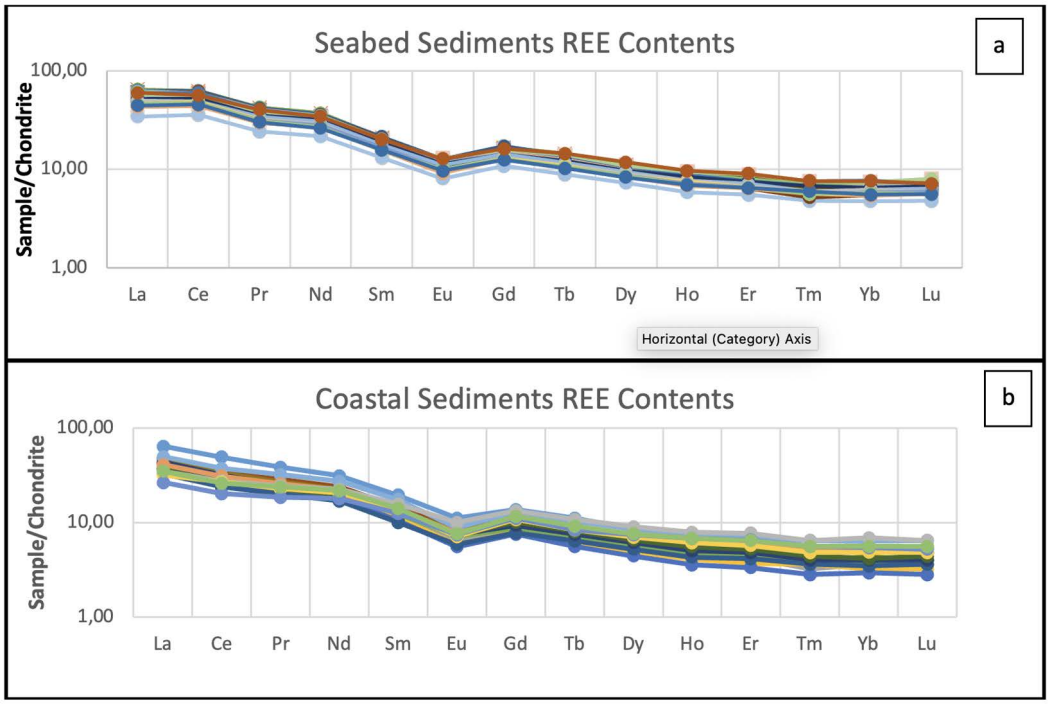

Figure 4. REE contents of the (a) Seabed sediments and (b) Coastal sediments

However, it is also recognized that in some settings positive Ce anomalies can arise from diagenetic processes, particularly the reductive dissolution of Fe–Mn (oxyhydr)oxides under suboxic to anoxic conditions (Bau et al., 1997). Coastal sediments, on the other hand, reflect more variable REE patterns with weaker or negative Ce anomalies, likely driven by dynamic depositional processes, fluctuating redox conditions, and greater input of detrital material from continental sources (Zhang et al., 2024; Sousa et al., 2022). Despite local differences in REE patterns between seabed and coastal samples, a pronounced negative europium anomaly (Eu/Eu < 1) was a pervasive feature across all analyzed samples. Such consistent Eu depletion is widely reported in modern sedimentary studies and is commonly attributed to provenance effects (e.g., plagioclase fractionation in source rocks) and selective mineral sorting during transport and deposition (Sousa et al., 2022; Ramos-Vázquez et al., 2021; Ruban et al., 2024; Li et al., 2024; Anenburg & Liu, 2024).

Major Oxide Elements Contents

Analysis of the major elements was performed on the sediment samples (seabed, n = 44; coastal, n = 18), presented in Table 2. The analysis reveals that SiO_2 is the dominant oxide, with concentrations ranging from 19.4% to 74.43%. Fe_2O_3 concentrations varied significantly, ranging from 4.09% to 18.66%, while Al_2O_3 was present between 3.38% and 15.53%. Based on the exploration report conducted by BBSPGL (2024), the analyzed samples are predominantly composed of clay minerals, which supports the interpretation that the presence of these minerals controls the variability in Al_2O_3 content. This observation is consistent with the well-established understanding that aluminosilicate clay minerals such as kaolinite, illite, and smectite serve as the primary hosts of aluminum in sedimentary environments, making Al_2O_3 a reliable indicator of clay abundance (Guan et al., 2023). Minor element oxides also displayed notable ranges: TiO_2 (0.44% to 2.19%), K_2O (0.29% to 2.78%), MgO (0.98% to 5.66%), MnO (0.04% to 0.28%), Na_2O (1% to 5.77%), and P_2O_5 (0.061% to 0.182%). Loss of Ignition (LOI) values spanned from 1.62% to 28%. Eventually, both Cr_2O_3 and S were consistently detected at trace levels, measuring less than 0.035%.

Based on the results of the Harker diagram plotting of the main oxide elements against Al_2O_3 (Figure 5), both negative and positive. These relationships indicate that some oxides decrease with increasing Al_2O_3, while others increase, reflecting different geochemical behavior during sediment formation. The strongest correlation is observed between Na_2O and Al_2O_3 (r =0.883), suggesting a strong positive association, whereas the weakest is between SiO_2 and Al_2O_3, showing a weak negative association (r = -0.006). Seabed sediments cluster tightly, indicating more stable environmental conditions and a relatively homogeneous source. In

Table 1. Chondrite-normalized REE contents and calculated parameters with following equations (1)–(5)

	SAMPLE ID																													
	SLL-003	SLL-004	SLL-006	SLL-007	SLL-008	SLL-010	SLL-011	SLL-012	SLL-015	SLL-016	SLL-018	SLL-019	SLL-021	SLL-022	SLL-027	SLL-030	SLL-031	SLL-034	SLL-038	SLL-039	SLL-042	SLL-043	SLL-044	SLL-046	SLL-048	SLL-055	SLL-068	SLL-082	SLL-083	SLL-089	SLL-090
La	13,2	14,3	14,5	14,7	14,1	15,4	15	14,7	14,1	11,8	14,4	14,1	14,8	13,3	13	13,7	12,8	14,4	14	12,3	13,2	11,8	12,9	12,7	8,17	13,2	12,1	12	12,5	13,6	11,7
Ce	32	36,3	34,7	36,8	36,1	38,3	38,4	37,6	36,3	30,6	36,8	36,7	36,1	33,2	33,6	34,4	33,4	36	36,3	32,2	34,5	30,7	34	33	21,9	34,1	31,2	31,2	32,9	34,7	30,7
Pr	3,63	3,83	3,84	3,93	3,74	4,11	4	3,92	3,77	3,18	3,87	3,77	3,9	3,56	3,56	3,63	3,47	3,78	3,75	3,34	3,59	3,2	3,52	3,45	2,33	3,56	3,29	3,27	3,44	3,69	3,2
Nd	15,3	15,9	15,8	16,2	15,7	17	16,5	16,2	15,7	13,3	15,9	15,6	16,1	14,6	14,8	15,1	14,5	15,9	15,5	14,2	14,9	13,5	14,6	14,5	9,91	14,8	13,7	13,9	14,5	15,7	13,4
Sm	3,05	3,19	3,06	3,17	3,13	3,22	3,27	3,16	3	2,66	3,03	3,06	3,11	2,85	2,88	3,01	2,84	3,07	3,05	2,75	2,86	2,63	2,84	2,92	2,01	2,88	2,65	2,77	2,79	3,02	2,66
Eu	0,71	0,7	0,69	0,74	0,71	0,73	0,74	0,71	0,71	0,58	0,71	0,69	0,7	0,63	0,63	0,68	0,63	0,71	0,7	0,61	0,65	0,58	0,65	0,65	0,47	0,67	0,61	0,64	0,66	0,75	0,6
Gd	3,31	3,3	3,23	3,27	3,22	3,33	3,42	3,26	3,13	2,66	3,18	3,14	3,12	2,92	2,93	3	2,77	3,16	3,18	2,78	2,95	2,69	2,85	2,86	2,16	2,92	2,79	2,81	2,88	3,15	2,62
Tb	0,5	0,51	0,5	0,51	0,5	0,52	0,5	0,51	0,48	0,41	0,49	0,49	0,48	0,44	0,46	0,46	0,45	0,48	0,48	0,42	0,44	0,41	0,45	0,44	0,32	0,45	0,41	0,42	0,43	0,51	0,41
Dy	2,87	2,86	2,77	2,91	2,73	2,86	2,88	2,86	2,69	2,31	2,75	2,7	2,6	2,5	2,58	2,58	2,46	2,71	2,65	2,45	2,46	2,29	2,53	2,48	1,86	2,51	2,37	2,4	2,46	2,77	2,34
Ho	0,53	0,52	0,51	0,53	0,52	0,51	0,52	0,52	0,49	0,42	0,5	0,49	0,48	0,45	0,47	0,47	0,44	0,5	0,49	0,44	0,45	0,41	0,46	0,45	0,33	0,46	0,43	0,43	0,45	0,53	0,44
Er	1,43	1,40	1,34	1,43	1,39	1,40	1,38	1,41	1,31	1,15	1,31	1,33	1,30	1,22	1,25	1,29	1,21	1,31	1,26	1,12	1,21	1,12	1,23	1,18	0,91	1,24	1,14	1,16	1,22	1,47	1,15
Tm	0,19	0,18	0,17	0,18	0,18	0,17	0,18	0,18	0,17	0,15	0,17	0,17	0,16	0,15	0,17	0,16	0,15	0,18	0,17	0,16	0,16	0,14	0,16	0,16	0,12	0,16	0,15	0,16	0,16	0,19	0,15
Yb	1,29	1,26	1,17	1,22	1,26	1,20	1,24	1,23	1,11	1,01	1,16	1,16	1,08	1,07	1,06	1,09	1,04	1,15	1,11	1,03	1,11	0,98	1,09	1,13	0,80	1,14	1,01	1,09	1,12	1,25	1,03
Lu	0,18	0,18	0,17	0,19	0,18	0,18	0,18	0,18	0,17	0,15	0,17	0,17	0,16	0,16	0,16	0,16	0,16	0,17	0,17	0,15	0,16	0,15	0,16	0,16	0,12	0,17	0,16	0,16	0,17	0,20	0,16
LREE	67,89	74,22	72,59	75,54	73,48	78,76	77,91	76,29	73,58	62,12	74,71	73,92	74,71	68,14	68,47	70,52	67,64	73,86	73,30	65,40	69,70	62,41	68,51	67,22	44,79	69,21	63,55	63,78	66,79	71,46	62,26
HREE	10,30	10,21	9,86	10,24	9,98	10,17	10,30	10,15	9,55	8,26	9,73	9,65	9,38	8,91	9,08	9,21	8,68	9,66	9,51	8,55	8,94	8,19	8,93	8,86	6,62	9,05	8,46	8,63	8,89	10,07	8,30
ΣREE	78,19	84,43	82,45	85,78	83,46	88,93	88,21	86,44	83,13	70,38	84,44	83,57	84,09	77,05	77,55	79,73	76,32	83,52	82,81	73,95	78,64	70,60	77,44	76,08	51,41	78,26	72,01	72,41	75,68	81,53	70,56
LREE/HREE	6,59	7,27	7,36	7,38	7,36	7,74	7,56	7,52	7,70	7,52	7,68	7,66	7,96	7,65	7,54	7,66	7,79	7,65	7,71	7,65	7,80	7,62	7,67	7,59	6,77	7,65	7,51	7,39	7,51	7,10	7,50
Eu/Eu*	0,67	0,65	0,66	0,69	0,67	0,67	0,67	0,67	0,70	0,66	0,69	0,67	0,68	0,66	0,65	0,68	0,68	0,69	0,68	0,66	0,67	0,66	0,69	0,68	0,68	0,70	0,67	0,69	0,70	0,73	0,68
Ce/Ce*	1,14	1,21	1,14	1,19	1,22	1,18	1,22	1,22	1,23	1,23	1,21	1,24	1,17	1,19	1,22	1,20	1,23	1,20	1,23	1,24	1,23	1,23	1,24	1,23	1,24	1,22	1,22	1,23	1,23	1,21	1,23
$(La/Yb)_N$	7,25	8,05	8,79	8,54	7,93	9,10	8,57	8,47	9,00	8,28	8,80	8,62	9,71	8,81	8,69	8,91	8,72	8,88	8,94	8,47	8,43	8,54	8,39	7,97	7,24	8,21	8,49	7,80	7,91	7,71	8,05
$(La/Sm)_N$	2,79	2,89	3,06	2,99	2,91	3,09	2,96	3,00	3,03	2,86	3,07	2,97	3,07	3,01	2,91	2,94	2,91	3,03	2,96	2,89	2,98	2,90	2,93	2,81	2,62	2,96	2,95	2,80	2,89	2,91	2,84
$(Gd/Yb)_N$	2,17	2,21	2,33	2,26	2,16	2,34	2,33	2,24	2,38	2,22	2,31	2,29	2,44	2,30	2,33	2,32	2,25	2,32	2,42	2,28	2,24	2,32	2,21	2,14	2,28	2,16	2,33	2,18	2,17	2,13	2,15

LREE (La, Ce, Pr, Nd, Sm, and Eu) ; HREE (Gd, Tb, Dy Ho, Er, Tm, and Lu)

(*Continued*)

	SAMPLE ID																													
	SLL-091	SLL-092	SLL-095	SLL-096	SLL-099	SLL-102	SLL-104	SLL-105	SLL-106	SLL-111	SLL-112	SLL-113	SLL-118	SML-01	SPL-01	SPL-02	SPL-02A	SPL-03	SPL-04	SPL-06	SPL-07	SPL-08	SPL-09	SPL-10	SPL-11	SPL-12	SPL-12A	SPL-13	SPL-14	SPL-15	SPL-16
La	10,3	10,7	12	12,3	11,5	11,8	10,2	11,8	11	11	11	10,6	14,3	15,1	10,2	9,23	8,91	8,7	9,96	7,73	11,2	9,97	11,3	10,3	8,7	11,7	9,63	8,22	7,53	6,29	8,24
Ce	27,5	28,2	30,8	32,2	30,2	30,2	27,1	29,6	29,9	28,8	28,9	28,1	34,7	30	19,3	17,2	16,7	15,9	19,4	14,5	20,5	18,8	20,4	19,5	17,3	22,9	18,9	16,8	16,5	12,4	15,9
Pr	2,87	2,97	3,34	3,41	3,15	3,28	2,87	3,1	3,06	3,01	3	2,91	3,86	3,68	2,49	2,17	2,14	2,1	2,34	1,92	2,73	2,45	2,58	2,36	2,16	3,07	2,46	2,33	2,17	1,78	2,28
Nd	12,3	12,6	13,9	14,5	13,2	13,9	12,2	13,3	12,7	12,8	12,3	12	15,8	14,3	9,83	8,54	8,47	8,22	9,17	7,73	10,9	9,82	10,2	9,4	8,96	12,4	10,1	10,3	9,31	8,17	9,89
Sm	2,5	2,46	2,71	2,88	2,63	2,73	2,38	2,56	2,47	2,57	2,4	2,41	3,09	2,97	2,06	1,71	1,69	1,61	1,89	1,52	2,23	2,03	2,04	1,96	1,94	2,67	2,08	2,39	2,02	1,91	2,15
Eu	0,56	0,56	0,62	0,66	0,61	0,64	0,53	0,58	0,57	0,58	0,58	0,56	0,74	0,64	0,4	0,37	0,34	0,32	0,41	0,34	0,49	0,43	0,48	0,43	0,43	0,51	0,45	0,58	0,41	0,43	0,44
Gd	2,51	2,53	2,75	2,85	2,73	2,85	2,52	2,6	2,59	2,48	2,52	2,5	3,25	2,74	1,9	1,59	1,56	1,49	1,73	1,54	2,15	1,89	1,98	1,86	2	2,56	2,13	2,63	2,15	2,21	2,31
Tb	0,38	0,39	0,43	0,44	0,42	0,42	0,38	0,4	0,39	0,38	0,38	0,37	0,52	0,4	0,26	0,24	0,22	0,2	0,26	0,23	0,32	0,29	0,3	0,27	0,29	0,37	0,3	0,39	0,3	0,3	0,33
Dy	2,16	2,2	2,41	2,48	2,37	2,41	2,15	2,31	2,18	2,19	2,19	2,11	3	2,15	1,43	1,36	1,24	1,12	1,45	1,32	1,8	1,62	1,7	1,56	1,65	2,17	1,81	2,28	1,77	1,88	1,92
Ho	0,4	0,4	0,45	0,47	0,43	0,43	0,38	0,43	0,42	0,4	0,39	0,39	0,54	0,41	0,27	0,25	0,23	0,2	0,26	0,24	0,33	0,31	0,31	0,28	0,31	0,41	0,36	0,44	0,34	0,38	0,38
Er	1,06	1,09	1,22	1,24	1,12	1,18	1,05	1,12	1,09	1,09	1,09	1,07	1,50	1,11	0,72	0,69	0,61	0,55	0,71	0,68	0,92	0,81	0,83	0,79	0,86	1,15	0,96	1,26	0,94	1,07	1,06
Tm	0,13	0,14	0,16	0,17	0,15	0,15	0,14	0,15	0,14	0,14	0,14	0,15	0,19	0,14	0,09	0,08	0,09	0,07	0,10	0,09	0,12	0,11	0,10	0,10	0,11	0,16	0,13	0,16	0,12	0,14	0,14
Yb	0,92	0,95	1,08	1,10	1,03	1,04	0,91	1,05	0,95	0,98	0,97	0,93	1,28	0,95	0,64	0,61	0,54	0,49	0,64	0,58	0,85	0,70	0,73	0,67	0,70	1,08	0,88	1,15	0,81	0,91	0,94
Lu	0,14	0,15	0,16	0,17	0,16	0,16	0,14	0,15	0,15	0,15	0,14	0,14	0,18	0,13	0,09	0,09	0,08	0,07	0,09	0,09	0,12	0,10	0,10	0,10	0,11	0,16	0,14	0,16	0,12	0,13	0,14
LREE	56,03	57,49	63,37	65,95	61,29	62,55	55,28	60,94	59,70	58,76	58,18	56,58	72,49	66,69	44,28	39,22	38,25	36,85	43,17	33,74	48,05	43,50	47,00	43,95	39,49	53,25	43,62	40,62	37,94	30,98	38,90
HREE	7,70	7,85	8,66	8,92	8,41	8,64	7,67	8,21	7,91	7,81	7,82	7,66	10,46	8,03	5,40	4,91	4,57	4,19	5,24	4,77	6,61	5,83	6,05	5,63	6,03	8,06	6,71	8,47	6,55	7,02	7,22
ΣREE	63,73	65,34	72,03	74,87	69,70	71,19	62,95	69,15	67,61	66,57	66,00	64,24	82,95	74,72	49,68	44,13	42,82	41,04	48,41	38,51	54,66	49,33	53,05	49,58	45,52	61,31	50,33	49,09	44,49	38,00	46,12
LREE/HREE	7,28	7,32	7,32	7,39	7,29	7,24	7,21	7,42	7,55	7,52	7,44	7,39	6,93	8,31	8,20	7,99	8,37	8,79	8,24	7,07	7,27	7,46	7,77	7,81	6,55	6,61	6,50	4,80	5,79	4,41	5,39
Eu/Eu*	0,67	0,68	0,68	0,69	0,68	0,69	0,65	0,68	0,68	0,69	0,71	0,69	0,70	0,67	0,61	0,68	0,63	0,62	0,68	0,67	0,67	0,66	0,72	0,68	0,66	0,59	0,64	0,70	0,59	0,63	0,59
Ce/Ce*	1,24	1,23	1,20	1,22	1,23	1,19	1,23	1,20	1,27	1,23	1,24	1,24	1,15	0,99	0,94	0,95	0,94	0,92	0,99	0,93	0,91	0,94	0,93	0,97	0,98	0,94	0,96	0,94	1,00	0,91	0,90
$(La/Yb)_N$	7,94	7,98	7,88	7,93	7,91	8,04	7,95	7,97	8,21	7,96	8,04	8,08	7,92	11,27	11,30	10,73	11,70	12,59	11,03	9,45	9,34	10,10	10,97	10,90	8,81	7,68	7,76	5,07	6,59	4,90	6,21
$(La/Sm)_N$	2,66	2,81	2,86	2,76	2,82	2,79	2,77	2,98	2,88	2,76	2,96	2,84	2,99	3,28	3,20	3,48	3,40	3,49	3,40	3,28	3,24	3,17	3,58	3,39	2,90	2,83	2,99	2,22	2,41	2,13	2,47
$(Gd/Yb)_N$	2,30	2,25	2,15	2,19	2,24	2,31	2,34	2,09	2,30	2,14	2,19	2,27	2,14	2,43	2,51	2,20	2,44	2,57	2,28	2,24	2,14	2,28	2,29	2,34	2,41	2,00	2,04	1,93	2,24	2,05	2,07

LREE (La, Ce, Pr, Nd, Sm, and Eu) ; HREE (Gd, Tb, Dy Ho, Er, Tm, and Lu)

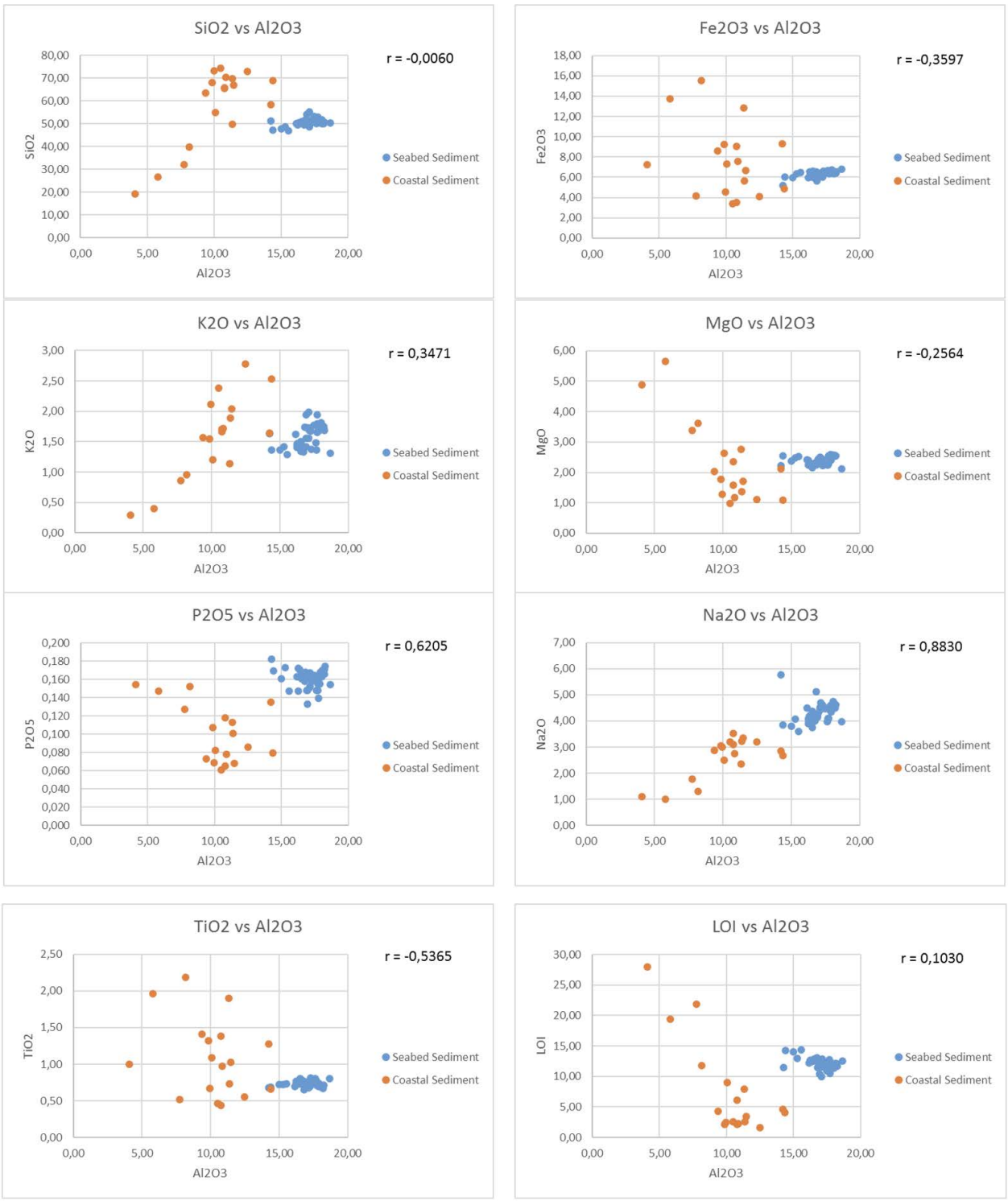

Figure 5. Harker diagram of Al_2O_3 vs selected major oxide elements

Table 2. Major oxides compositions (%) and some elemental ratios along with calculated weathering indices according to equations (8)-(11)

	SAMPLE ID																														
	SLL-003	SLL-004	SLL-006	SLL-007	SLL-008	SLL-010	SLL-011	SLL-012	SLL-015	SLL-016	SLL-018	SLL-019	SLL-021	SLL-022	SLL-027	SLL-030	SLL-031	SLL-034	SLL-038	SLL-039	SLL-042	SLL-043	SLL-044	SLL-046	SLL-048	SLL-055	SLL-068	SLL-082	SLL-083	SLL-089	SLL-090
SiO2	53,20	50,54	55,28	51,65	50,55	53,03	51,14	50,12	50,14	51,57	50,73	50,18	54,08	51,29	49,84	51,54	51,18	51,71	51,42	50,89	51,40	50,05	48,76	50,81	51,33	50,29	49,56	50,51	46,97	50,41	50,55
Al2O3	17,47	18,26	17,11	18,03	18,21	17,74	17,87	18,19	18,07	16,80	17,71	18,13	16,92	17,13	17,16	16,94	17,21	17,76	17,86	17,24	17,72	16,16	17,12	16,91	14,25	17,62	16,25	17,30	15,55	18,66	16,90
Fe2O3	6,47	6,52	6,23	6,49	6,40	6,35	6,44	6,41	6,36	5,65	6,38	6,40	6,20	6,36	6,18	6,40	6,02	6,46	6,40	6,05	6,39	5,96	6,25	6,33	5,22	6,68	6,57	6,62	6,47	6,81	6,30
TiO2	0,74	0,71	0,75	0,71	0,70	0,72	0,70	0,67	0,69	0,65	0,71	0,70	0,73	0,71	0,68	0,73	0,69	0,75	0,74	0,70	0,77	0,70	0,73	0,75	0,68	0,80	0,77	0,81	0,73	0,80	0,76
CaO	1,95	2,72	1,74	2,44	2,84	2,29	2,91	3,05	2,94	3,77	2,81	3,00	2,83	3,39	3,71	3,55	3,92	2,57	2,85	4,17	2,78	5,35	4,58	4,41	6,07	3,35	5,45	3,85	7,28	3,01	4,86
K2O	1,77	1,69	1,99	1,81	1,72	1,94	1,79	1,75	1,74	1,74	1,79	1,72	1,94	1,73	1,69	1,73	1,72	1,68	1,69	1,68	1,65	1,62	1,56	1,56	1,63	1,48	1,41	1,38	1,29	1,31	1,42
MgO	2,26	2,54	2,29	2,52	2,55	2,51	2,60	2,55	2,57	2,24	2,54	2,56	2,38	2,51	2,45	2,45	2,44	2,42	2,40	2,45	2,28	2,41	2,45	2,35	2,22	2,24	2,39	2,22	2,53	2,12	2,30
MnO	0,10	0,12	0,10	0,12	0,11	0,11	0,12	0,11	0,11	0,10	0,10	0,10	0,08	0,09	0,10	0,09	0,09	0,09	0,09	0,10	0,09	0,10	0,10	0,08	0,11	0,08	0,10	0,08	0,08	0,08	0,09
Na2O	4,47	4,62	4,50	4,60	4,63	4,47	4,60	4,49	4,74	5,11	4,49	4,54	4,26	4,53	4,69	4,29	4,62	4,48	4,41	4,62	4,09	4,51	4,43	4,23	5,77	3,98	3,90	4,59	3,61	3,98	4,14
P2O5	0,16	0,17	0,15	0,16	0,17	0,16	0,16	0,17	0,17	0,17	0,16	0,17	0,13	0,15	0,16	0,15	0,16	0,14	0,16	0,16	0,15	0,16	0,17	0,15	0,18	0,15	0,15	0,16	0,15	0,15	0,16
Cr2O3	0,02	<0,01	<0,01	<0,01	<0,01	<0,01	0,01	<0,01	<0,01	0,02	<0,01	0,01	<0,01	<0,01	<0,01	<0,01	0,01	<0,01	<0,01	<0,01	<0,01	0,01	0,01	<0,01	0,03	<0,01	0,01	<0,01	<0,01	<0,01	0,17
S	0,31	0,28	0,23	0,25	0,31	0,27	0,33	0,34	0,29	0,25	0,27	0,31	0,23	0,26	0,26	0,22	0,25	0,43	0,27	0,26	0,27	0,24	0,24	0,24	0,22	0,24	0,21	0,22	0,20	0,24	0,23
LOI	10,91	11,70	9,93	11,38	12,02	10,53	11,49	12,12	12,14	11,47	11,64	12,16	10,45	11,79	12,54	11,43	11,61	11,56	11,67	11,87	11,48	12,20	12,89	12,05	11,42	12,30	12,61	12,40	14,41	12,53	12,36
Total	99,80	99,90	100,00	100,00	100,00	100,00	100,00	100,00	100,00	99,50	99,30	100,00	100,00	100,00	99,50	99,50	100,00	100,00	100,00	100,00	99,10	99,50	99,30	99,90	99,10	99,20	99,40	100,00	99,30	100,00	100,00
K2O/Na2O	0,40	0,37	0,44	0,39	0,37	0,43	0,39	0,39	0,37	0,34	0,40	0,38	0,46	0,38	0,36	0,40	0,37	0,38	0,38	0,36	0,40	0,36	0,35	0,37	0,28	0,37	0,36	0,30	0,36	0,33	0,34
Al2O3/TiO2	23,61	25,72	22,81	25,39	26,01	24,64	25,53	27,15	26,19	25,85	24,94	25,90	23,18	24,13	25,24	23,21	24,94	23,68	24,14	24,63	23,01	23,09	23,45	22,55	20,96	22,03	21,10	21,36	21,30	23,33	22,24
SiO2/Al2O3	3,05	2,77	3,23	2,86	2,78	2,99	2,86	2,76	2,77	3,07	2,86	2,77	3,20	2,99	2,90	3,04	2,97	2,91	2,88	2,95	2,90	3,10	2,85	3,00	3,60	2,85	3,05	2,92	3,02	2,70	2,99
log (K2O/Na2O)	-0,40	-0,44	-0,35	-0,41	-0,43	-0,36	-0,41	-0,41	-0,44	-0,47	-0,40	-0,42	-0,34	-0,42	-0,44	-0,39	-0,43	-0,43	-0,42	-0,44	-0,39	-0,44	-0,45	-0,43	-0,55	-0,43	-0,44	-0,52	-0,45	-0,48	-0,46
log (Al2O3/TiO2)	1,37	1,41	1,36	1,40	1,42	1,39	1,41	1,43	1,42	1,41	1,40	1,41	1,37	1,38	1,40	1,37	1,40	1,37	1,38	1,39	1,36	1,36	1,37	1,35	1,32	1,34	1,32	1,33	1,33	1,37	1,35
log (SiO2/Al2O3)	0,48	0,44	0,51	0,46	0,44	0,48	0,46	0,44	0,44	0,49	0,46	0,44	0,50	0,48	0,46	0,48	0,47	0,46	0,46	0,47	0,46	0,49	0,45	0,48	0,56	0,46	0,48	0,47	0,48	0,43	0,48
CIA	73,68	74,32	72,5	73,77	74,14	73,46	73,66	74,46	73,6	71,04	73,82	74,33	73,18	73,24	72,9	73,78	73,08	74,25	74,54	73,24	75,53	72,5	74,08	74,49	65,82	76,34	75,37	74,34	76,04	77,91	75,24
PIA	77,84	78,2	77,06	77,91	78,08	77,95	77,76	78,55	77,5	74,67	78	78,33	77,86	77,27	76,74	78	77,03	78,21	78,57	77,11	79,71	76,33	77,84	78,4	68,62	80,22	79,19	77,62	79,8	81,34	78,9
CIW	79,63	79,81	79,18	79,67	79,73	79,87	79,53	80,2	79,22	76,68	79,77	79,97	79,89	79,09	78,54	79,79	78,84	79,86	80,2	78,87	81,25	78,18	79,44	79,99	71,18	81,57	80,65	79,03	81,16	82,42	80,32
ICV	0,905	0,887	0,927	0,901	0,885	0,908	0,909	0,879	0,897	0,922	0,904	0,884	0,921	0,93	0,92	0,926	0,905	0,894	0,881	0,905	0,862	0,947	0,907	0,905	1,097	0,866	0,932	0,908	0,946	0,809	0,888

CaO* is the CaO value that has been corrected based on Mc Lennan (1990)

(*continued*)

	SAMPLE ID																													
	SLL-091	SLL-092	SLL-095	SLL-096	SLL-099	SLL-102	SLL-104	SLL-105	SLL-106	SLL-111	SLL-112	SLL-113	SLL-118	SML-01	SPL-01	SPL-02	SPL-02A	SPL-03	SPL-04	SPL-06	SPL-07	SPL-08	SPL-09	SPL-10	SPL-11	SPL-12	SPL-12A	SPL-13	SPL-14	SPL-15	SPL-16
SiO2	47,13	48,69	49,61	50,18	50,27	50,10	47,92	50,01	50,34	50,51	50,68	50,94	51,38	68,80	72,78	63,52	73,31	74,43	66,87	65,52	65,77	69,87	68,11	70,26	54,98	58,32	49,91	26,76	39,85	19,14	32,05
Al2O3	14,40	15,29	16,74	17,68	16,34	16,52	15,01	16,25	16,28	16,55	16,51	16,53	17,91	14,37	12,49	9,37	9,97	10,50	11,46	10,78	10,77	11,38	9,86	10,87	10,07	14,23	11,34	5,81	8,16	4,09	7,75
Fe2O3	6,03	6,36	6,54	6,58	6,12	6,61	5,97	6,12	6,04	6,28	6,03	5,99	6,73	4,84	4,12	8,59	4,54	3,38	6,67	3,51	9,05	5,61	9,26	7,57	7,32	9,33	12,82	13,71	15,53	7,22	4,17
TiO2	0,69	0,72	0,78	0,79	0,73	0,80	0,72	0,74	0,73	0,75	0,73	0,73	0,73	0,66	0,55	1,41	0,67	0,46	1,03	0,44	1,38	0,73	1,32	0,97	1,09	1,28	1,90	1,96	2,19	1,00	0,52
CaO	9,08	6,76	5,20	4,21	5,48	5,57	7,71	5,30	5,34	4,95	4,67	4,80	2,45	1,05	1,42	5,53	2,61	2,20	3,33	6,91	3,66	3,35	2,90	2,55	11,12	5,46	9,85	24,77	15,52	33,22	26,67
K2O	1,37	1,42	1,33	1,36	1,46	1,34	1,37	1,46	1,47	1,43	1,47	1,50	1,71	2,53	2,78	1,57	2,11	2,38	2,04	1,66	1,71	1,89	1,55	1,72	1,20	1,64	1,14	0,40	0,96	0,29	0,86
MgO	2,54	2,48	2,31	2,24	2,31	2,26	2,38	2,25	2,24	2,23	2,16	2,17	2,42	1,09	1,11	2,03	1,29	0,98	1,72	1,59	2,35	1,37	1,77	1,17	2,63	2,11	2,75	5,66	3,62	4,89	3,39
MnO	0,10	0,10	0,09	0,09	0,09	0,09	0,09	0,09	0,09	0,09	0,09	0,09	0,11	0,07	0,07	0,10	0,06	0,04	0,09	0,07	0,12	0,08	0,12	0,10	0,15	0,13	0,17	0,28	0,23	0,21	0,13
Na2O	3,84	4,07	3,99	4,10	4,20	3,76	3,80	4,07	4,15	4,15	4,38	4,30	4,34	2,68	3,21	2,88	3,00	3,21	3,34	3,52	3,11	3,23	3,05	2,76	2,50	2,84	2,34	1,00	1,30	1,10	1,78
P2O5	0,17	0,17	0,16	0,16	0,17	0,16	0,16	0,16	0,17	0,17	0,16	0,17	0,17	0,08	0,09	0,07	0,07	0,06	0,07	0,07	0,12	0,10	0,11	0,08	0,08	0,14	0,11	0,15	0,15	0,15	0,13
Cr2O3	0,02	0,01	<0,01	<0,01	0,02	<0,01	0,02	<0,01	0,01	0,01	0,01	<0,01	0,02	0,01	0,01	<0,01	0,02	0,01	0,02	0,02	0,02	0,01	0,01	0,01	<0,01	<0,01	<0,01	<0,01	0,02	<0,01	0,02
S	0,18	0,18	0,26	0,22	0,19	0,19	0,19	0,20	0,18	0,20	0,23	0,22	0,27	0,01	<0,002	0,04	0,03	0,03	0,03	0,04	0,02	0,01	0,02	<0,002	0,05	0,03	0,05	0,09	0,07	0,11	0,09
LOI	14,27	13,02	13,04	12,75	12,41	12,71	14,03	12,66	12,54	12,91	12,53	12,63	11,45	4,09	1,62	4,34	2,44	2,59	3,45	6,11	2,19	2,64	2,13	2,23	9,06	4,68	7,89	19,38	11,82	28,00	21,88
Total	99,80	99,30	100,00	100,00	99,80	100,00	99,30	99,30	99,60	100,00	99,70	100,00	99,70	100,00	100,00	99,50	100,00	100,00	100,00	100,00	100,00	100,00	100,00	100,00	100,00	100,00	100,00	100,00	99,40	99,40	99,40
K2O/Na2O	0,36	0,35	0,33	0,33	0,35	0,36	0,36	0,36	0,35	0,34	0,34	0,35	0,39	0,94	0,87	0,55	0,70	0,74	0,61	0,47	0,55	0,59	0,51	0,62	0,48	0,58	0,49	0,40	0,74	0,26	0,48
Al2O3/TiO2	20,87	21,24	21,46	22,38	22,38	20,65	20,85	21,96	22,30	22,07	22,62	22,64	24,53	21,77	22,71	6,65	14,88	22,83	11,13	24,50	7,80	15,59	7,47	11,21	9,24	11,12	5,97	2,96	3,73	4,09	14,90
SiO2/Al2O3	3,27	3,18	2,96	2,84	3,08	3,03	3,19	3,08	3,09	3,05	3,07	3,08	2,87	4,79	5,83	6,78	7,35	7,09	5,84	6,08	6,11	6,14	6,91	6,46	5,46	4,10	4,40	4,61	4,88	4,68	4,14
log (K2O/Na2O)	-0,45	-0,46	-0,48	-0,48	-0,46	-0,45	-0,44	-0,45	-0,45	-0,46	-0,47	-0,46	-0,40	-0,03	-0,06	-0,26	-0,15	-0,13	-0,21	-0,33	-0,26	-0,23	-0,29	-0,21	-0,32	-0,24	-0,31	-0,40	-0,13	-0,58	-0,32
log (Al2O3/TiO2)	1,32	1,33	1,33	1,35	1,35	1,31	1,32	1,34	1,35	1,34	1,35	1,35	1,39	1,34	1,36	0,82	1,17	1,36	1,05	1,39	0,89	1,19	0,87	1,05	0,97	1,05	0,78	0,47	0,57	0,61	1,17
log (SiO2/Al2O3)	0,51	0,50	0,47	0,45	0,49	0,48	0,50	0,49	0,49	0,48	0,49	0,49	0,46	0,68	0,77	0,83	0,87	0,85	0,77	0,78	0,79	0,79	0,84	0,81	0,74	0,61	0,64	0,66	0,69	0,67	0,62
CIA	73,43	73,58	75,88	76,4	74,27	76,41	74,38	74,61	74,34	74,79	73,84	74,03	74,75	73,39	67,59	67,8	66,11	65,26	68,05	67,54	69,08	68,97	68,19	70,81	73,13	76,06	76,52	80,58	78,31	74,64	74,59
PIA	77,24	77,31	79,43	79,92	77,99	80,15	78,21	78,42	78,11	78,46	77,45	77,75	78,87	81,54	75,15	73,03	72,38	71,67	73,82	72,15	74,45	74,61	73,15	76,83	78,01	81,59	81,34	84,4	84,71	77,55	79,47
CIW	78,95	78,98	80,75	81,18	79,55	81,46	79,8	79,97	79,69	79,95	79,03	79,36	80,49	84,28	79,55	76,49	76,87	76,59	77,43	75,38	77,59	77,89	76,37	79,75	80,11	83,36	82,89	85,32	86,26	78,81	81,32
ICV	1,012	0,991	0,898	0,857	0,912	0,9	0,955	0,906	0,904	0,902	0,9	0,894	0,896	0,826	1,062	2,36	1,432	1,205	1,59	1,642	1,985	1,429	2,025	1,549	2,583	1,602	2,731	8,224	4,822	11,72	4,841

CaO* is the CaO value that has been corrected based on Mc Lennan (1990)

contrast, coastal sediments show scattered and irregular distributions, reflecting the influence of variable physical processes such as wave action, currents, and fluctuating terrigenous input. This observation is consistent with previous studies reporting that coastal sediments generally exhibit higher geochemical variability than deeper marine sediments due to stronger continental and oceanographic controls (e.g., Morton, 2002; Garzanti et al., 2018).

DISCUSSION

Provenance

The provenance analysis of seabed and coastal sediments from the Limau Waters area was conducted using two geochemical approaches: the discriminant function diagram by Roser & Korsch (1988) and the TiO_2 versus Zr plot by Hayashi et al. (1997), in order to better constrain the nature of the source rocks. The discriminant function diagram (Figure 6), which utilizes multiple major oxide elements (TiO_2, Al_2O_3, Fe_2O_3, MgO, CaO, Na_2O, and K_2O), indicates that the seabed sediments predominantly plot within the intermediate igneous provenance field, with several samples extending toward the mafic domain. In contrast, coastal sediments are more widely scattered, with several samples plotting within the felsic igneous field and others extending into the recycled/mature quartzose sedimentary provenance area. This suggests that coastal sediments were derived from a more mixed and possibly reworked source, which may include older continental or volcanic materials (Cullers, 1994; Roser & Korsch, 1988).

The TiO_2 vs Zr plot (Figure 7), which focuses on magmatic differentiation trends, shows that most seabed sediment samples cluster within the felsic igneous rock field, characterized by relatively low TiO_2 content and enriched Zr values. This distribution may reflect the presence of resistant heavy minerals such as zircon, typically concentrated during sedimentary sorting processes from felsic sources (Hayashi et al., 1997; McLennan et al., 1993). On the other hand, coastal sediments are primarily plotted in the mafic to intermediate igneous fields, indicating higher TiO_2 content and suggesting a more direct input from mafic volcanic rocks, likely of local origin.

The apparent discrepancy between the two diagrams can be explained by the different sensitivities and focuses of each method. The discriminant function diagram is more robust in identifying general provenance trends because it integrates multiple major elements, and is thus less sensitive to grain size effects or mineral sorting (Gaspar et al., 2022; Nagarajan et al., 2023). In contrast, TiO_2–Zr (or TiO_2 vs. Zr) diagrams are particularly sensitive to the selective enrichment of resistant heavy minerals (e.g., zircon, rutile,

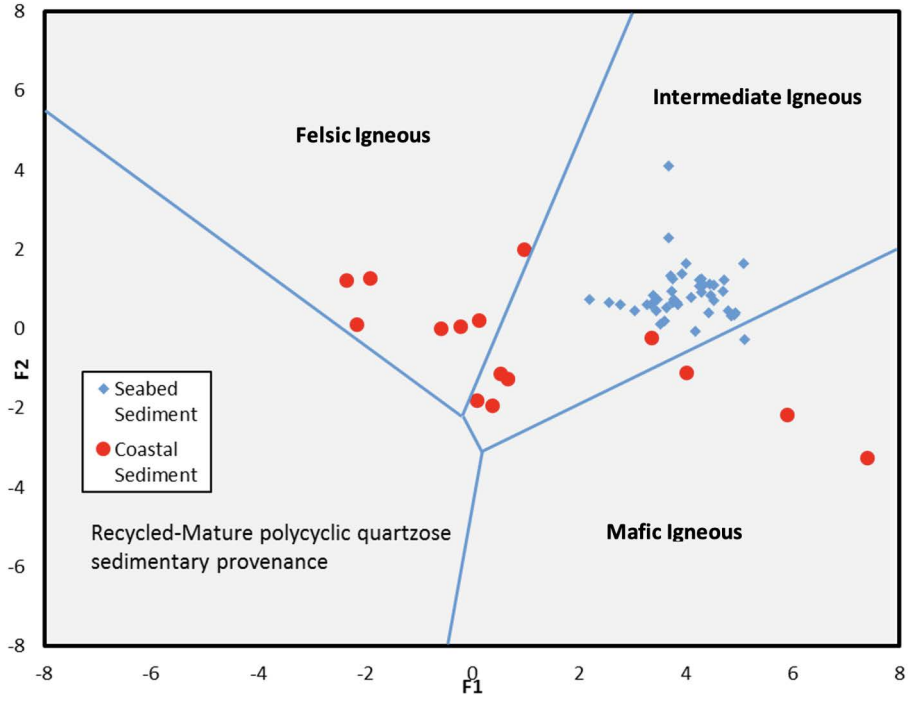

Figure 6. Provenance Discriminant Function Diagram (Roser and Korsch, 1988) with following equation (6) and (7)

ilmenite); hydrodynamic concentration or reworking of these minerals can artificially shift Ti–Zr systematics and bias provenance interpretation toward more felsic signatures (Patias et al., 2024).

Taken together, these results suggest that the seabed sediments are largely derived from intermediate to felsic volcanic sources, possibly influenced by offshore inputs and the enrichment of heavy minerals, while the coastal sediments reflect a more heterogeneous provenance, involving mafic volcanic input and reworked continental or sedimentary material. These interpretations are consistent with the regional geology of the Limau coastal area, which comprises both Tertiary and Quaternary volcanic rocks, including andesitic, basaltic, and rhyolitic lithologies (Irzon, 2020). It also accordance with the regional geological conditions and rock outcrops found in the field, where in the Limau mainland area and its surroundings according to Amin et al. (1993) is predominantly composed of the Hulusimpang volcanic rock formation with some granite intrusion rocks. The Hulusimpang Formation is an Oligocene-Miocene volcanic rock formation consisting of volcanic breccia, lava, and tuff with andesitic - basaltic composition. Meanwhile, the Miocene granite intrusion is an igneous rock that cut through the Hulusimpang Formation. This rock is a felsic intrusive rock with local distribution. It appears that the seabed sediment at the study area has more potential to contain sulfide minerals compared to coastal sediment, because of their correlation to the Hulusimpang Formation.

Paleoweathering and sediment maturity

The paleoweathering conditions and sediment maturity of the seabed and coastal sediments in the Limau Waters area were evaluated using a two-dimensional CIA–ICV plot that integrates geochemical indices reflecting weathering intensity and sediment maturity (Figure 8). This type of plot is commonly constructed using the Chemical Index of Alteration (CIA) and the Index of Compositional Variability (ICV), following the approaches of Nesbitt & Young (1982), and Cox et al. (1995). The vertical axis at approximately CIA = 70 separates weakly weathered (CIA < 70) from intensely weathered (CIA > 70) source terrains (Nesbitt & Young, 1982).

The majority of both seabed and coastal sediment samples fall within the weak weathering field, suggesting limited chemical alteration, likely due to derivation from volcanic or young arc-related sources with minimal exposure to prolonged tropical weathering. A subset of coastal samples, however, lies beyond the CIA = 70 threshold, suggesting contribution from more weathered or older continental sources (McLennan, 1993).

Sediment maturity in Limau Waters area is inferred from the horizontal axis at ICV = 1, where values <1 indicate mature sediments (quartz-rich and compositionally stable), while values >1 reflect immature sediments (feldspar- or mafic-rich, less altered) (Cox et al., 1995). The results show that Seabed sediments cluster mostly fall near or just

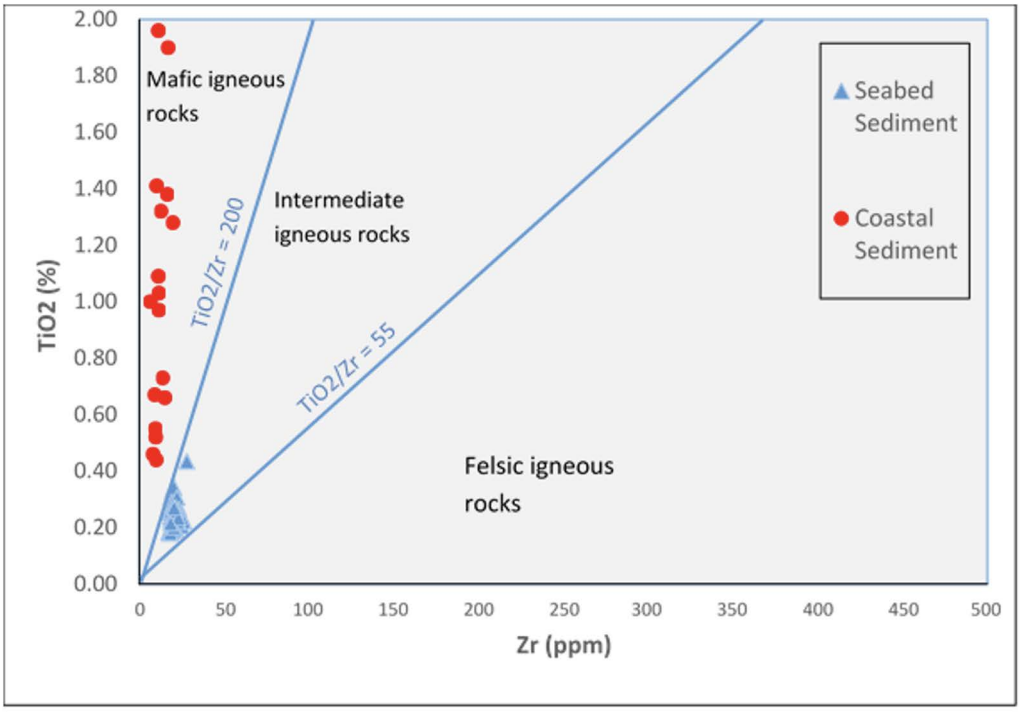

Figure 7. TiO_2 vs Zr plot (Hayashi et al., 1997)

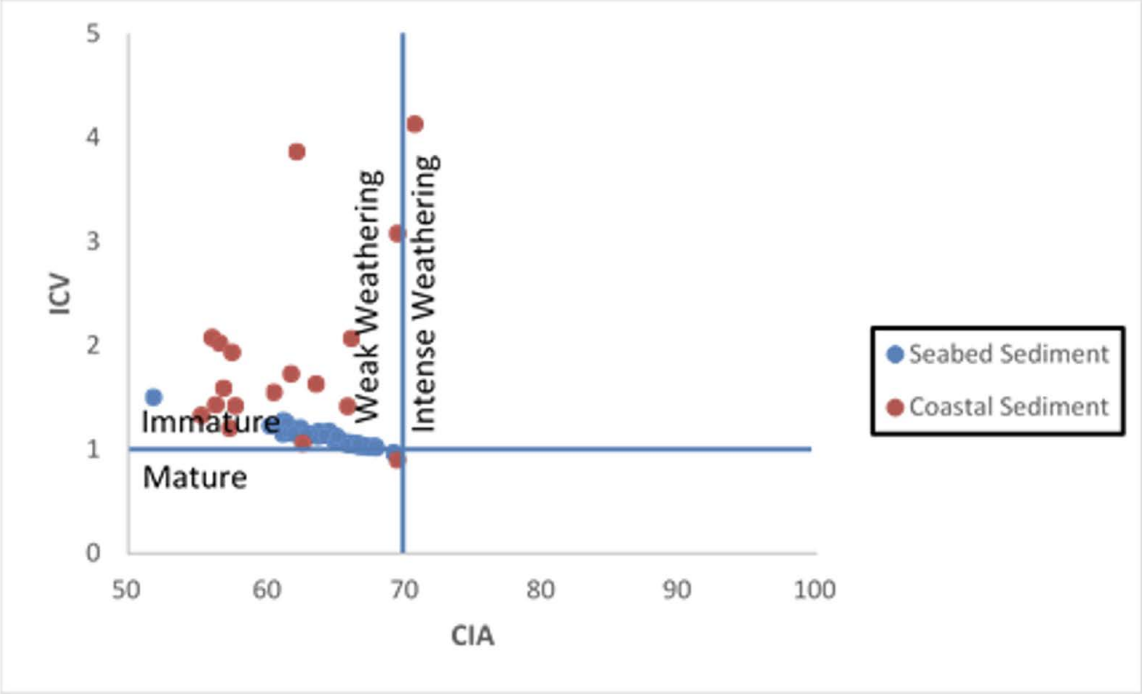

Figure 8. ICV vs CIA diagram (Nesbit and Young 1984; Cox et al. 1995)

below the ICV = 1, implying a dominance of stable mineral components and possible sedimentary reworking or recycling. Meanwhile, Coastal sediments predominantly fall into the immature field, consistent with derivation from first-cycle volcanic sources, with minimal transport or chemical weathering.

The seabed sediments, being more compositionally mature, likely underwent longer transport or offshore reworking, resulting in enrichment of stable mineral phases such as quartz and depletion of labile elements. In contrast, the coastal sediments retain the signature of proximal volcanic sources, characterized by limited chemical weathering and short transport distances, consistent with active arc settings. These findings complement the provenance interpretations derived from major element discrimination diagrams (Hayashi et al., 1997; Roser & Korsch, 1988), in which seabed sediments show felsic to intermediate igneous affinities, while coastal sediments exhibit stronger mafic volcanic signatures.

CONCLUSSIONS

The integration of provenance and geochemical weathering–maturity data reveals distinct differences in the sedimentary characteristics of seabed and coastal sediments in the Limau Waters area. These differences reflect variations in source rock composition, weathering intensity, and depositional processes. Provenance analysis indicates that seabed sediments are predominantly derived from intermediate to felsic igneous sources, as evidenced by their low TiO_2 and relatively high Zr contents. This suggests possible contributions from felsic volcanic rocks and enrichment of resistant heavy minerals such as zircon. In contrast, coastal sediments display a geochemical affinity toward mafic to intermediate igneous sources, likely reflecting direct input from nearby Quaternary volcanic rocks. Paleoweathering and maturity analysis-supports this distinction. Seabed sediments are generally geochemically mature (ICV < 1) and exhibit low chemical weathering intensity (CIA < 70), indicating a stable mineralogical composition possibly resulting from longer transport or sedimentary reworking. Coastal sediments, on the other hand, are immature (ICV > 1) and more compositionally variable, with a few samples showing signs of moderate to intense chemical weathering (CIA > 70), suggesting limited transport and derivation from less altered, first-cycle volcanic sources. Together, the data suggest that seabed sediments have undergone more extensive geochemical stabilization and sedimentary processing, while coastal sediments represent more proximal and compositionally diverse inputs, reflecting the active volcanic geology of the region. These findings provide a comprehensive

understanding of sediment dispersal and source rock contributions in the Limau Waters area.

ACKNOWLEDGEMENTS

The authors sincerely acknowledge the support and facilitation provided by the Head of the Marine Geological Institute, Ministry of Energy and Mineral Resources of the Republic of Indonesia. We are also deeply grateful to all members of the Marine Geological Institute survey team whose dedication, technical assistance, and collaborative spirit have significantly contributed to the completion of this scientific work. Their efforts during field surveys, sample processing, data analysis, and insightful discussions were essential to the success of this study.

REFERENCES

Advokaat, E. L., Bonger, M. L. M., Rudyawan, A., BouDagher-Fadhel, M. K., Langereis, C. G., & van Hinsbergen, D. J. J., 2018. Early Cretaceous origin of the Woyla Arc, Sumatra. *Earth and Planetary Science Letters, 498,* 348–361.

Anenburg, M., & Liu, Y., 2024. A Global Marine Sediment Compilation and a Cerium Anomaly Perspective on Metasomatized Mantle Sources for REE-Mineralized Carbonatites. Journal of Geophysical Research: Solid Earth, 129(7), e2023JB028546. https://doi.org/10.1029/2023JB028546

Amin, T. C., Sidarto, Santosa, S., & Gunawan, W., 1993. *Peta geologi bersistem lembar Kotaagung skala 1:250.000.* Pusat Penelitian dan Pengembangan Geologi, Departemen Pertambangan dan Energi.

Barber, A. J., & Crow, M. J., 2005. Structure and structural history. In A. J. Barber, M. J. Crow, & J. S. Milsom (Eds.), *Sumatra: Geology, resources, and tectonic evolution* (Geological Society Memoir No. 31, pp. 295–310). Geological Society, London.

Bau, M., Möller, P., & Dulski, P., 1997. Yttrium and lanthanides in eastern Mediterranean seawater and their fractionation during redox-cycling. Marine Chemistry, 56(1-2), 123-131. https://doi.org/10.1016/S0304-4203(96)00091-6

BBSPGL., 2024. *Laporan Survei Prospeksi Mineral Letakan Emas (Au Placer) Di Perairan Limau Dan Sekitarnya, Teluk Semangko, Provinsi Lampung.* Balai Besar Survei dan Pemetaan Geologi Kelautan. [Internal report, unpublished].

Cox, R., Lowe, D. R., & Cullers, R. L., 1995. The influence of sediment recycling and basement composition on evolution of mudrock chemistry in the southwestern United States. *Geochimica et Cosmochimica Acta, 59*(14), 2919–2940. https://doi.org/10.1016/0016-7037(95)00185-9

Crow, M. J., & van Leeuwen, T. M., 2005. Metallic mineral deposits. In A. J. Barber, M. J. Crow, & J. S. Milsom (Eds.), *Sumatra: Geology, resources and tectonic evolution* (Geological Society Memoir No. 31, pp. 147–174). Geological Society, London.

Cruz, A., Dinis, P. A., Gomes, A., & Leite, P., 2021. Influence of sediment cycling on the rare-earth element geochemistry of fluvial deposits. *Geosciences, 11*(9), 384. https://doi.org/10.3390/geosciences11090384

Cullers, R. L., 1994. The controls on the major and trace element evolution of shales, siltstones, and sandstones of Ordovician to Tertiary age in the western United States. *Chemical Geology, 114,* 297–323.

Darlan, Y., 1997. Sedimen permukaan dasar laut sebagai perangkap endapan emas letakan di perairan Teluk Semangko, Lampung Selatan. In *Proceedings of the Indonesian Geologists Association at the XXVI Annual Scientific Meeting* (pp. 913–922). Jakarta.

Ekoa Bessa, A. Z., Ndjigui, P. D., Fuh, G. C., Armstrong-Altrin, J. S., & Betsi, T. B., 2021. Mineralogy and geochemistry of the Ossa Lake Complex sediments, Southern Cameroon: Implications for paleoweathering and provenance. *Arabian Journal of Geosciences, 14,* 322. https://doi.org/10.1007/s12517-021-06646-3

Fedo, C. M., Nesbitt, H. W., & Young, G. M., 1995. Unraveling the effects of potassium metasomatism in sedimentary rocks and paleosols, with implications for paleoweathering conditions and provenance. *Geology, 23,* 921–924.

Garzanti, E., Resentini, A., & Andò, S., 2018. Provenance of passive-margin sand (southern Africa). *Journal of Sedimentary Research*, 88(1), 47–64.

Gaspar, L., Blake, W. H., Lizaga, I., Latorre, B., & Navas, A., 2022. Particle size effect on geochemical composition of experimental soil mixtures relevant for unmixing modelling. *Geomorphology*, *403*, 108178. https://doi.org/10.1016/j.geomorph.2022.108178

Guan, Y., Chen, Y., Sun, X., Xu, L., Xu, D., Zhu, Z., & He, W., 2023. The Clay Mineralogy and Geochemistry of Sediments in the Beibu Gulf, South China Sea: A Record of the Holocene Sedimentary Environmental Change. *Journal of Marine Science and Engineering*, *11*(7), 1463. https://doi.org/10.3390/jmse11071463

Hayashi, K. I., Fujisawa, H., Holland, H. D., & Ohmoto, H., 1997. Geochemistry of ~1.9 Ga sedimentary rocks from northeastern Labrador, Canada. *Geochimica et Cosmochimica Acta, 61,* 4115–4137.

Harnois, L., 1988. The CIW index: A new chemical index of weathering. *Sedimentary Geology, 55,* 319–322.

Irzon, R., 2020. Komparasi geokimia batuan gunung api Kuarter dan Tersier di Tepian Selatan Lampung. Eksplorium, 41(2), 101–114. https://doi.org/10.17146/eksplorium.2020.41.2.6053

Li, X., Ge, J., Zhao, X., Qi, K., Jones, B. G., & Fang, X., 2024. Geochemistry of Quaternary sediments in the northwestern South China Sea: Sediment provenance and mid-Pleistocene transition. *Marine Geology*, *477*, 107371. https://doi.org/10.1016/j.margeo.2024.107371

McDonough, W. F., & Sun, S. -s., 1995. The composition of the Earth. Chemical Geology, 120(3), 223–253. https://doi.org/https://doi.org/10.1016/0009-2541(94)00140-4

McLennan, S. M., 1989. Rare earth elements in sedimentary rocks: Influence of provenance and sedimentary processes. In B. R. Lipin & G. A. McKay (Eds.), Geochemistry and mineralogy of rare earth elements (Reviews in Mineralogy, Vol. 21, pp. 169–200). Mineralogical Society of America. https://doi.org/10.1515/9781501509032-010

McLennan, S. M., Hemming, S. R., McDaniel, D. K., & Hanson, G. N., 1993. Geochemical approaches to sedimentation, provenance, and tectonics. In Processes *controlling the composition of clastic sediments* (Geological Society of America Special Paper 284, pp. 21–40). Geological Society of America.

Metcalfe, I., 2017. Tectonic evolutions of Sundaland. *Bulletin of the Geological Society of Malaysia, 63,* 27–60. https://doi.org/10.7186/bgsm63201702

Morton, A. C., 2002. Provenance indicators and their value in sedimentary petrology. In: *Provenance of Arenites* (pp. 113–142). Springer, Dordrecht.

Muksin, I., & Heditama, D. M., 2016. *Laporan eksplorasi umum endapan zeolit Kecamatan Limau, Kabupaten Tanggamus Provinsi Lampung.* Pusat Sumber Daya Mineral, Batubara dan Panas Bumi. [Internal report, unpublished].

Nagarajan, R., Eswaramoorthi, S. G., Anandkumar, A., & Ramkumar, M., 2023. Geochemical fractionation, mobility of elements and environmental significance of surface sediments in a Tropical River, Borneo. *Marine Pollution Bulletin*, *192*, 115090. https://doi.org/10.1016/j.marpolbul.2023.115090

Nesbitt, H. W., & Young, G. M., 1982. Early Proterozoic climates and plate motions inferred from major element chemistry of lutites. *Nature, 299,* 715–717. https://doi.org/10.1038/299715a0

Nesbitt, H. W., & Young, G. M., 1984. Prediction of some weathering trends of plutonic and volcanic rocks based on thermodynamic and kinetic considerations. *Geochimica et Cosmochimica Acta, 48,* 1523–1534.

Patias, D., Zhou, R., Aitchison, J. C., Cluzel, D., Ireland, T., Lian, D., & Yang, J., 2024. Beyond zircon fingerprinting: Zircon and TiO2 polymorphs constrain genealogy and evolution of the New Caledonian ophiolite. Chemical Geology, 644, 121841. https://doi.org/10.1016/j.chemgeo.2023.121841

Ramos-Vázquez, M.A., Armstrong-Altrin, J.S. Provenance of sediments from Barra del Tordo and Tesoro beaches, Tamaulipas State, northwestern Gulf of Mexico. J. Palaeogeogr. 10, 20, 2021. https://doi.org/10.1186/s42501-021-00101-4

Roser, B. P., & Korsch, R. J., 1988. Provenance signatures of sandstone–mudstone suites determined using discriminant function analysis of major-element data. *Chemical Geology, 67,* 119–139.

Ruban, A., Dudarev, O., Rudmin, M., & Semiletov, I., 2024. Rare Earth Elements in Sediments from the Laptev Sea Shelf: Insight into Sources and Distribution Factors. *Quaternary*, *7*(1), 12. https://doi.org/10.3390/quat7010012

Sousa, T. A., Venancio, I. M., Marques, E. D., Figueiredo, T. S., Nascimento, R. A., Smoak, J. M., Albuquerque, A. L., Valeriano, C. M., & Vieira, E., 2022. REE Anomalies Changes in Bottom Sediments Applied in the Western Equatorial Atlantic Since the Last Interglacial. *Frontiers in Marine Science*, *9*, 846976. https://doi.org/10.3389/fmars.2022.846976

Sukardjono, H., Kurnio, H., Hardjawidjaksana, K., Lugra, I. W., Silitonga, F., & Budiman., 1990. *Laporan penyelidikan geologi dan geofisika di kawasan Kompleks Teluk Semangko, Lampung Selatan.* Pusat Pengembangan Geologi Kelautan. [Internal report, unpublished].

Taylor, S. R., & McLennan, S. M., 1985. *The Continental Crust: Its Composition and Evolution*. Oxford: Blackwell.

Zhang, K., & Shields, G. A., 2022. Sedimentary Ce anomalies: Secular change and implications for paleoenvironmental evolution. Earth-Science Reviews, 229, 104015. https://doi.org/10.1016/j.earscirev.2022.104015

Zhang, Y., Zhang, Z., Stephenson, W., & Chen, Y., 2024. Geochemical Behavior of Rare Earth Elements in Tidal Flat Sediments from Qidong Cape, Yangtze River Estuary: Implications for the Study of Sedimentary Environmental
Change. *Land*, *13*(9), 1425. https://doi.org/10.3390/land13091425